Available online at www.sciencedirect.com
SCIENCE DIRECT
Polymer 46 (2005) 4743–4752
polymer
www.elsevier.com/locate/polymer

Miscibility and viscoelastic properties of acrylic polyhedral oligomeric silsesquioxane–poly(methyl methacrylate) blends

Edward T. Kopesky[a], Timothy S. Haddad[b], Gareth H. McKinley[c,*], Robert E. Cohen[a,*]

[a]Department of Chemical Engineering, Massachusetts Institute of Technology, 77 Massachusetts Ave, Cambridge, MA 02139, USA
[b]ERC Inc., Air Force Research Laboratory, Edwards AFB, CA 93524, USA
[c]Department of Mechanical Engineering, Massachusetts Institute of Technology, Cambridge, MA 02139, USA

Received 14 January 2005; accepted 1 April 2005
Available online 22 April 2005

Abstract

We investigate the miscibility of acrylic polyhedral oligomeric silsesquioxanes (POSS) [characteristic size $d \approx 2$ nm] and poly(methyl methacrylate)(PMMA) in order to determine the effect of well-dispersed POSS nanoparticles on the thermomechanical properties of PMMA. Two different acrylic POSS species (unmodified and hydrogenated) were blended separately with PMMA at volume fractions up to $\phi = 0.30$. Both POSS species have a plasticizing effect on PMMA by lowering the glass transition temperature T_g and decreasing the melt-state linear viscoelastic moduli measured in small amplitude oscillatory shear flow. The unmodified acrylic-POSS has better miscibility with PMMA than the hydrogenated form, approaching complete miscibility for loadings $\phi < 0.10$. At a loading $\phi = 0.05$, the unmodified acrylic POSS induces a 4.9 °C decrease in the T_g of PMMA, far less than the 17.4 °C decrease in the glass transition temperature observed in a blend of 5 vol% dioctyl phthalate (DOP) in PMMA; however, the decrease in the glass transition temperature per added plasticizer molecule is nearly the same in the unmodified acrylic-POSS–PMMA blend compared with the DOP–PMMA blend. Time-temperature superposition (TTS) was applied successfully to the storage and loss moduli data and the resulting shift factors were correlated with a significant increase in free volume of the blends. The fractional free volume $f_0 = 0.046$ for PMMA at $T_0 = 170$ °C while for a blend of 5 vol% unmodified acrylic-POSS in PMMA $f_0 = 0.057$, which corresponds to an addition of 0.47 nm^3 per added POSS molecule at $\phi = 0.05$. The degree of dispersion was characterized using both wide-angle X-ray diffraction (WAXD) and dynamic mechanical analysis (DMA). Diffraction patterns for both blend systems show clear evidence of phase separation at $\phi = 0.20$ and higher, but no significant phase separation is evident at $\phi = 0.10$ and lower. The storage modulus measured in DMA indicates appreciable phase separation for unmodified acrylic POSS loadings $\phi \geq 0.10$, while no evidence of phase separation is present in the $\phi = 0.05$ blend in DMA.

Keywords: POSS; Plasticization; Nanocomposites

1. Introduction

Polymers filled with very small nanoparticles ($d <$ 15 nm) have been studied in great detail both theoretically and experimentally in recent years and a number of unusual results have been reported [1–8]. While conventional fillers ($d \geq 50$ nm) reinforce polymer matrices regardless of the polymer–particle interaction, nanoparticles have shown the ability to either reinforce or plasticize polymer matrices depending on their size and the interfacial interaction between the polymer and the nanoparticle. Roberts et al. [5] reported the effect of particle size in silicate particle–poly(dimethyl siloxane) blends. Very small particles ($d =$ 0.7 nm) reduced the viscosity of poly(dimethyl siloxane) while larger silicate particles ($d = 4.4$ nm) increased the viscosity. Mackay et al. [3] further demonstrated the effect of very small size by blending crosslinked poly(styrene) particles ($d =$ 6–10 nm) with linear poly(styrene). They reported as much as a 70% decrease in viscosity with the addition of nanoparticles and also a decrease in the glass transition temperature T_g. Zhang and Archer [6] reported the dramatic effect that polymer–particle interactions have on polymer–nanoparticle rheology. They observed solid-like

* Corresponding authors.
E-mail addresses: ed_k@mit.edu (E.T. Kopesky), timothy.haddad@edwards.af.mil (T.S. Haddad), gareth@mit.edu (G.H. McKinley), recohen@mit.edu (R.E. Cohen).

0032-3861/$ - see front matter © 2005 Elsevier Ltd. All rights reserved.
doi:10.1016/j.polymer.2005.04.001

behavior in the linear viscoelastic properties of poly(ethylene oxide) when bare silica nanoparticles ($d=12$ nm) were added at a volume fraction of only $\phi=0.02$, but there was no effect on the rheological properties when the polymer–nanoparticle interaction was essentially athermal. Starr et al. [7,8] performed a computational study that simulated a polymer chain near a nanoparticle ($d=10$ nm) and calculated cases for which the polymer–nanoparticle interaction was either attractive or non-attractive. For the attractive case, the glass transition temperature T_g increased by approximately 6% for a particle loading of 8 wt% while for the non-attractive case the T_g decreased by a similar amount at the same loading. McCoy et al. [4] reported similar results for polymers in confined geometries.

A class of nanoparticles that has drawn significant attention recently are polyhedral oligomeric silsesquioxanes (POSS). They are hybrid organic-inorganic nanoparticles with a cage structure R_xT_x, where R represents an organic group on each corner, T represents the silsequinoxane linkage ($SiO_{1.5}$), and x commonly has values of 8, 10, or 12. An $R_{10}T_{10}$ POSS cage ($d\approx2$ nm) with acrylic R-groups is shown in Fig. 1(a). In light of the recent work on polymer–nanoparticle systems, the hybrid structure of POSS particles, with a silica core and a variable organic shell, offers a precise way to vary the polymer–nanoparticle interaction and thereby achieve either plasticization or reinforcement, depending on the application. A wide variety of studies have been carried out on POSS-containing copolymers and POSS–homopolymer blends [9], probing their thermal [10–17], morphological [10,13,14,17–25], mechanical [21,23,24,26,27], and self-assembly [10,28] properties. The rheological behavior of POSS-filled homopolymers has been studied by us [13] and by others [29]. In both cases, the POSS filler tended to phase separate into microcrystallites, even at loadings as small as $\phi=0.01$. Despite this phase separation, we observed a slight decrease in the viscosity for loadings $\phi<0.05$ [13]. This decrease was attributed to a small amount of molecularly-dispersed POSS particles that plasticized the matrix in the melt state at small loadings; however we did not observe a decrease in either T_g or an increase in the fractional free volume f_0, which would be expected if plasticization were occurring.

The difficulty in suppressing crystallization of the POSS fillers when dispersed in homopolymers led to the selection of a non-crystallizable POSS species for the present study. To further improve the dispersion in PMMA, two POSS species with acrylic R-groups were chosen. One contained pendant carbon–carbon double bonds [pictured in Fig. 1(a)] and the other was hydrogenated to reduce the carbon–carbon double bonds to single bonds.

2. Experimental section

2.1. Materials

The polymer used in the present study was a commercial poly(methyl methacrylate)(PMMA) resin obtained from

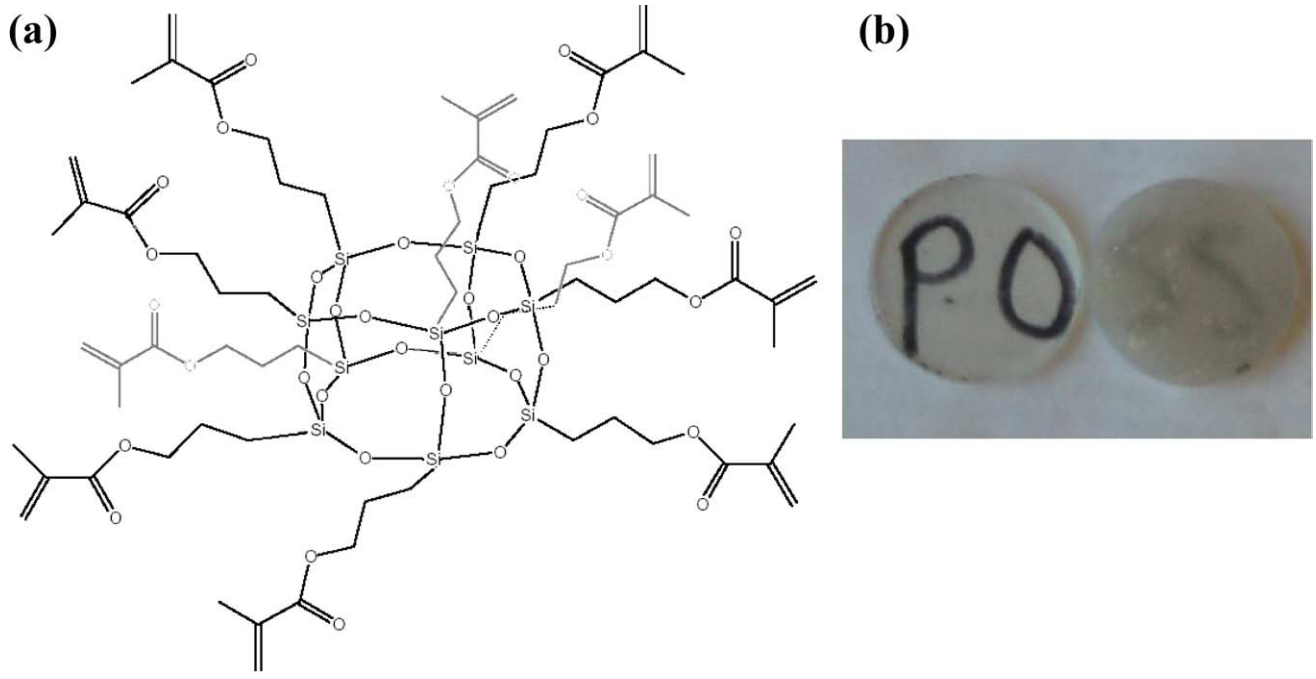

Fig. 1. (a) Chemical structure of the unmodified acrylic-POSS used in the study. The hydrogenated form was the same except for the absence of any pendant carbon–carbon double bonds. (b) Comparison of clarity of two blends containing 20 vol% acrylic-POSS in PMMA. The clearer sample on the left contains the unmodified POSS pictured in (a); the opaque sample on the right contains the hydrogenated form of the POSS in (a) that contains no carbon–carbon double bonds.

Atofina Chemicals (Atoglas V920) with a weight average molecular weight $M_w = 80{,}200$ g/mol and a polydispersity $M_w/M_n = 1.7$. The PMMA was blended with two similar but distinct acrylic-POSS species: the first contained methacryloxypropyl R-groups (Hybrid Plastics Methacryl-POSS) and was used as received, the second was a hydrogenated form of the first that contained no carbon–carbon double bonds. Both types of POSS were mixtures of T_8, T_{10}, T_{12}, and T_{14} cages, with the T_{10} cages being the majority component ($\approx$47 wt% as measured by ^{29}Si NMR). The chemical structure of a T_{10} cage of the unmodified acrylic-POSS is pictured in Fig. 1. Both types of acrylic-POSS had a density $\rho = 1.19$ g/cm^3.

2.2. Hydrogenation of (methacryloxypropyl)$_n$(SiO$_{3/2}$)$_n$

In a glass-lined PARR pressure vessel, 13 g of (methacryloxypropyl)$_n$(SiO$_{3/2}$)$_n$ (hybrid plastics) was dissolved in 50 ml of dry toluene along with 50 mg of 5% palladium on carbon catalyst (Aldrich). The reactor was pressurized to 500 psi of hydrogen gas and heated to 70 °C for 14 h. After cooling to room temperature, the reactor was reduced to atmospheric pressure and the solution was filtered through a short pad of silica to remove the catalyst. Removal of the toluene solvent produced the thick viscous product. Proton NMR spectroscopy showed the complete removal of starting material olefinic protons at 6.0 and 5.5 ppm. ^{1}H NMR ($CDCl_3$ referenced to residual $CHCl_3$ at 7.26 ppm) 3.99 (mult, 2H, CH_2O), 2.50 (sept, $^3J_{H-H} = 6.8$ Hz, 1H, CH), 1.67 (mult, 2H, $CH_2CH_2CH_2$), 1.12 (d, $^3J_{H-H} = 6.8$ Hz, 6H, CH_3), 0.63 (mult, 2H, $SiCH_2$). ^{13}C{^{1}H} NMR ($CDCl_3$ referenced at 77.0 ppm; multiple peaks are observed due to the presence of a variety of POSS cages sizes with $n = 10$ and 12 the most abundant) 176.92 and 176.89 (C=O), 65.86 and 65.81 (OCH_2), 33.84 (CH), 22.35 and 22.22 ($CH_2CH_2CH_2$), 18.91 (CH_3), 9.02 and 8.50 ($SiCH_2$). ^{29}Si{^{1}H} NMR (referenced to external $SiMe_4$ at 0 ppm) −65.6, −66.6 (T_8), −67.5, −67.6, −67.7, −67.8, −68.1, −68.2 (T_{12}), −68.5 (T_{10}), −70.9 (T_{12}).

2.3. Solution blending and sample preparation

Blends were prepared by dissolving PMMA and acrylic-POSS at approximately 10 wt% in THF at room temperature. The solutions were poured into a partially-covered petri dish and the solvent was evaporated over a period of 24 h. The cast films were then further dried in a vacuum oven at 110 °C for 48 h. Lower temperatures were insufficient to remove all of the solvent. Samples for rheological and dynamic mechanical analysis were molded in a Carver press at a temperature $T = 190$ °C.

2.4. Thermal and morphological characterization

The blends were characterized using both differential scanning calorimetry (DSC) and dynamic mechanical analysis (DMA). The DSC tests were performed on a TA Instruments Q1000. Samples were heated to $T \geq T_g + 50$ °C at a rate of 5 °C/min, cooled to $T = -90$ °C at the same rate, and data were collected on the second heating ramp at 5 °C/min. Glass transition temperatures T_g were determined from the inflection point in the heat flow versus temperature curves. The DMA measurements were carried out on a TA Instruments Q800 using rectangular samples ($50 \times 12 \times 3$ mm^3) in a three-point bending geometry. Samples were cooled to $T = -80$ °C and held for 5 min before being subsequently heated to $T = 150$ °C at a rate of 3 °C/min.

Wide angle X-ray diffraction (WAXD) was performed on a Rigaku RU300 18 kW rotating anode generator with a 250 mm diffractometer. Tests were carried out at 23 °C using Cu K_α radiation.

2.5. Rheological characterization

Rheological tests were performed on a TA Instruments AR2000 controlled-stress rheometer. Samples were tested between 25 mm parallel plates in small amplitude oscillatory shear flow at strains between 0.1 and 2%. The average gap separation was 2 mm. Master curves of the storage modulus G' and the loss modulus G'' were generated using horizontal shift factors a_T determined from the loss tangent $\tan\delta = G''/G'$ over the temperature range 125 °C $\leq T \leq$ 210 °C. Subsequent vertical shift factors b_T were required to account for changes in density and variations in the gap separation with temperature.

3. Results and discussion

3.1. Differential scanning calorimetry

In Fig. 2(a) we plot differential scanning calorimetry (DSC) curves for the unmodified acrylic-POSS–PMMA blends. Loadings up to $\phi = 0.30$ lead to a decrease in the glass transition temperature T_g and a broadening of the glass transition region. In the $\phi = 0.30$ blend, a second glass transition event appears at $T = -55$ °C. This corresponds to the T_g of the pure POSS and indicates significant phase separation at this loading. This is also the point at which optical clarity of the unmodified acrylic-POSS blends is lost. The curve for the pure acrylic-POSS in Fig. 2(a) shows the beginning of a large endotherm at $T = 120$ °C. This is due to crosslinking initiated by the pendant carbon–carbon double bonds on the corners of the acrylic-POSS cages. The only measured composition to show evidence of this crosslinking in DSC was $\phi = 0.30$, which showed a very shallow endotherm beginning slightly above $T = 150$ °C, just outside the range of the data plotted in Fig. 2.

In Fig. 2(b) we show DSC curves for the hydrogenated form of the acrylic-POSS in PMMA. A similar trend of decreasing glass transition temperature T_g with increasing POSS loading is observed, however the drop in T_g is less

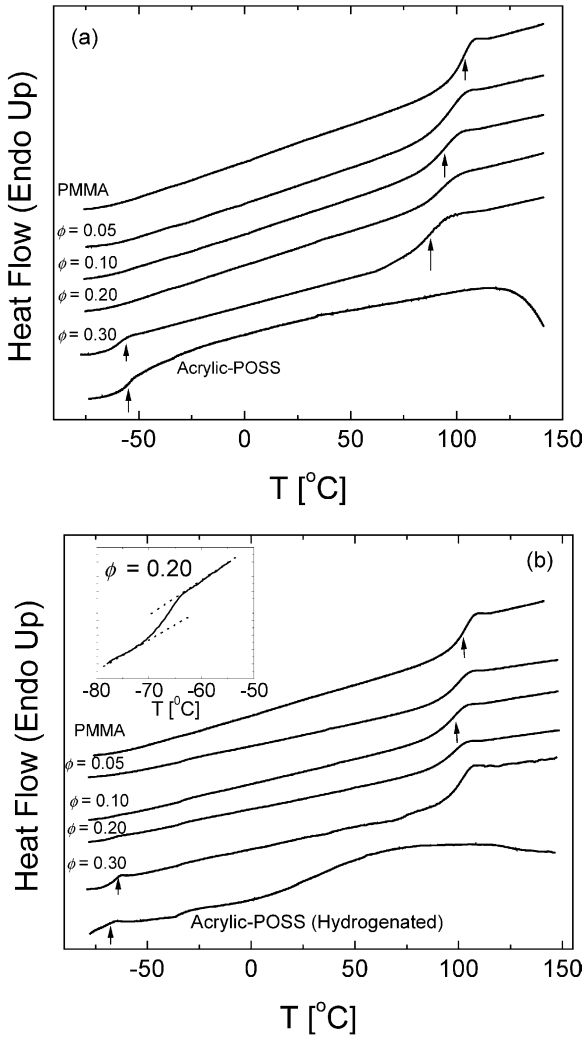

Fig. 2. DSC curves for (a) unmodified acrylic-POSS in PMMA and (b) hydrogenated acrylic-POSS in PMMA. The inset in (b) is a close-up of the low-T region of the 20 vol% blend, showing evidence of phase separation.

substantial in the hydrogenated system. The decreased plasticization is also accompanied by much lower optical clarity when compared with the unmodified acrylic-POSS–PMMA blends at comparable POSS volume fractions. A comparison between the $\phi = 0.20$ blends in both the unmodified and the hydrogenated systems is shown in Fig. 1(b). The unmodified POSS blend is nearly transparent and the hydrogenated blend is almost completely opaque. The hint of a second T_g due to phase separation is present in the $\phi = 0.20$ hydrogenated blend at $T \approx -68$ °C [see inset to Fig. 2(b)] and becomes obvious in the $\phi = 0.30$ blend. No sharp endotherm at temperatures above 150 °C is observed in the hydrogenated POSS, nor in any of the blends, indicating that crosslinking does not occur in this system.

The values of the glass transition temperatures T_g extracted from the DSC scans in Fig. 2 are plotted in Fig. 3 for both the unmodified and the hydrogenated acrylic-POSS–PMMA blends. The magnitude of the drop in T_g is always larger in the unmodified acrylic-POSS–PMMA

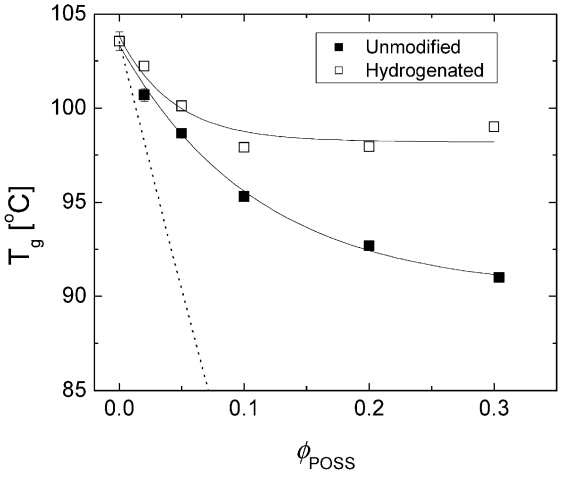

Fig. 3. Glass transition temperatures measured in DSC for both types of acrylic-POSS–PMMA blends. The dotted line represents the prediction of the Fox equation (Eq. (1)).

system, and the difference grows progressively greater at higher loadings. The hydrogenated acrylic-POSS ceases to plasticize further the PMMA matrix above $\phi = 0.10$, whereas at $\phi = 0.20$ the unmodified acrylic-POSS continues to induce a modest decrease in T_g. For comparison, the well-known Fox equation [30] has also been plotted as the dotted line in Fig. 3:

$$\frac{1}{T_g} = \frac{\phi}{T_{g,POSS}} + \frac{(1-\phi)}{T_{g,PMMA}} \tag{1}$$

where $T_{g,PMMA}$ and $T_{g,POSS}$ are the pure component glass transition temperatures of the PMMA (104 °C) and the unmodified acrylic-POSS (−55 °C).

Neither blend system follows the prediction of the Fox equation; however, each system does have an approximately linear decrease in T_g at loadings $\phi \leq 0.10$ and they therefore follow the common relation for polymer-plasticizer blends at low concentrations of plasticizer [31]

$$T_g = T_{g,PMMA} - k\phi \tag{2}$$

where k is a constant that typically ranges from 200 to 500 °C for plasticized polystyrene blends. By fitting the values of T_g at $\phi \leq 0.05$, k values of 98 and 50 °C are obtained for the unmodified and the hydrogenated acrylic-POSS–PMMA blends, respectively. These k values are well below the expected range for conventional plasticizers. It is likely that the relatively larger sizes of the POSS molecules ($V_{POSS} = 1297$ cm^3/mol) compared with conventional plasticizers may be a primary cause for this disparity in k values. For comparison, we added dioctyl phthalate (DOP, $V_{DOP} = 403$ cm^3/mol) to PMMA. At a DOP concentration $\phi = 0.05$, the measured T_g was 86.1 °C and at $\phi = 0.10$ the T_g was 71.6 °C, corresponding to a k value of 320 °C, or approximately 3.2 times that observed in the unmodified acrylic-POSS–PMMA blends. At a plasticizer loading of $\phi = 0.05$, the actual number density of added plasticizer

particles is much larger in the DOP–PMMA blend (1.26×10^{-4} mol/cm^3 of blend) than in the unmodified acrylic-POSS–PMMA blend (0.39×10^{-4} mol/cm^3 of blend). Therefore, adding 3.2 times as many DOP molecules per unit volume as acrylic-POSS molecules resulted in a comparably enhanced reduction in the T_g (reflected in the coefficient k in Eq. (2)) beyond that observed in the acrylic-POSS–PMMA blend. Therefore the lower degree of plasticization observed in the unmodified acrylic-POSS–PMMA blends at low loadings ($\phi\leq0.10$) is a result of the larger size of the POSS molecules which, at a given volume fraction, leads to far fewer added POSS cages than in the DOP–PMMA blend. Consequently there is relatively less polymer–particle contact over which free volume can be generated in a POSS-modified blend, and hence the T_g reduction is correspondingly reduced.

3.2. Wide angle X-ray diffraction

Wide angle X-ray diffraction (WAXD) was used to further characterize the miscibility of the acrylic-POSS–PMMA blends. Diffraction patterns for the unmodified and the hydrogenated acrylic-POSS systems are shown in Fig. 4(a) and (b), respectively. The characteristics of the WAXD patterns for the two blend systems are similar at comparable loadings of POSS. In each case, the $\phi=0.05$ and $\phi=0.10$ diffraction patterns have only a broad amorphous peak at $2\theta\approx14°$, corresponding to the amorphous PMMA matrix peak. At $\phi=0.20$, a shoulder matching the high-angle amorphous peak of the acrylic-POSS at $2\theta\approx19.3°$ appears, and becomes more prominent at $\phi=30$. This corresponds to a spacing $d=0.46$ nm, which is within the range $d=0.4$–0.5 nm at which crystallizable POSS species and POSS-containing copolymers show a strong secondary peak [13,18–20,25]. Broad peaks at $2\theta=6.56°$ in the $\phi=0.20$ unmodified POSS blend and $2\theta=6.40°$ in the $\phi=0.20$ hydrogenated POSS blend correspond to the low angle amorphous peaks in the pure POSS spectra. A spacing of $d=1.35$ nm for the unmodified T_{10} acrylic-POSS molecule of molecular weight 1544 g/mol is a reasonable center-to-center spacing; this would correspond to a mass density of 1.04 g/cm^3 if the POSS were arranged on a simple cubic lattice (SC) and a mass density of 1.47 g/cm^3 for a face-centered cubic lattice (FCC). The actual density of the non-crystalline acrylic-POSS at room temperature is 1.19 g/cm^3, comfortably between the sparse SC limit and the close-packed FCC limit.

We would expect to see a shift in the location of the amorphous peak of the PMMA ($2\theta=14.1°$) if indeed POSS particles were distributed throughout the matrix. The nanoparticles would be expected to push chains apart and shift the peak to a higher d spacing (smaller 2θ angle). However, the POSS present in the blends tends to shift slightly the locations of the PMMA matrix peaks at loadings $\phi=0.05$ and $\phi=0.10$ in Fig. 4 to higher 2θ values. This is a consequence of the overlapping signal of the POSS centered

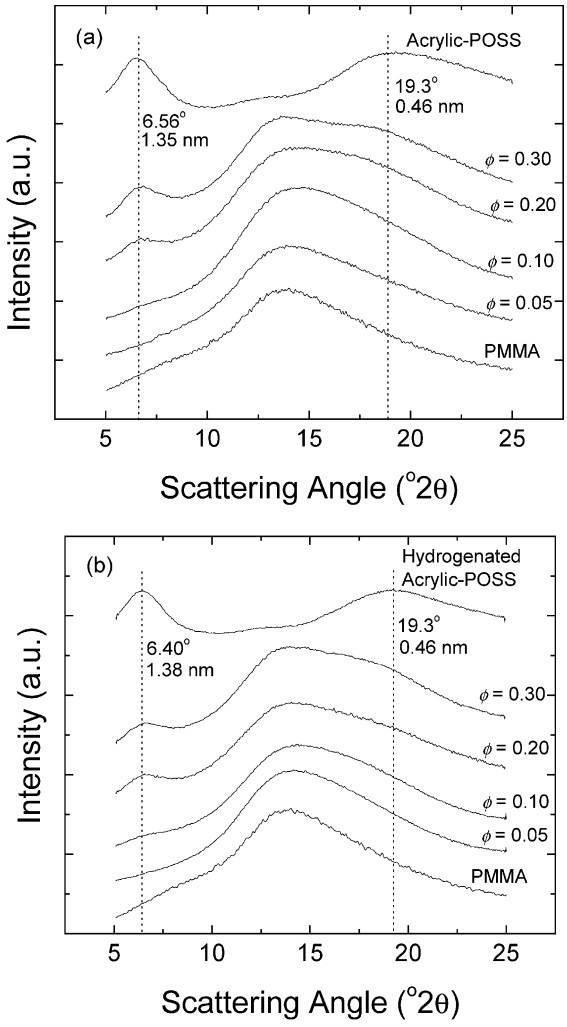

Fig. 4. WAXD spectra for (a) unmodified acrylic-POSS in PMMA and (b) hydrogenated acrylic-POSS in PMMA.

at $2\theta=19.3°$. This does not allow the precise location of the matrix peak to be determined in these blends. However, the matrix peak and the POSS peak begin to separate at $\phi=0.20$ in both Fig. 4(a) and (b); at $\phi=0.30$ it is possible to see both peaks. In the unmodified acrylic-POSS–PMMA blend spectra in Fig. 4(a) at $\phi=0.30$, the matrix peak location is $2\theta=13.8°$ ($d=0.641$ nm), while in the hydrogenated blends in Fig. 4(b) at $\phi=0.30$ the matrix peak location is $2\theta=14.0°$ ($d=0.632$ nm). These are both larger d spacings than in the pure PMMA ($d=0.627$ nm), indicating penetration of the POSS nanoparticles between the PMMA chains. As expected, the unmodified acrylic-POSS [Fig. 4(a)], which is more miscible than the hydrogenated form, shows a larger shift in the amorphous peak location.

3.3. Rheology

In Figs. 5 and 6, we plot master curves of the storage and loss moduli for PMMA filled respectively with unmodified and hydrogenated acrylic-POSS at a reference temperature

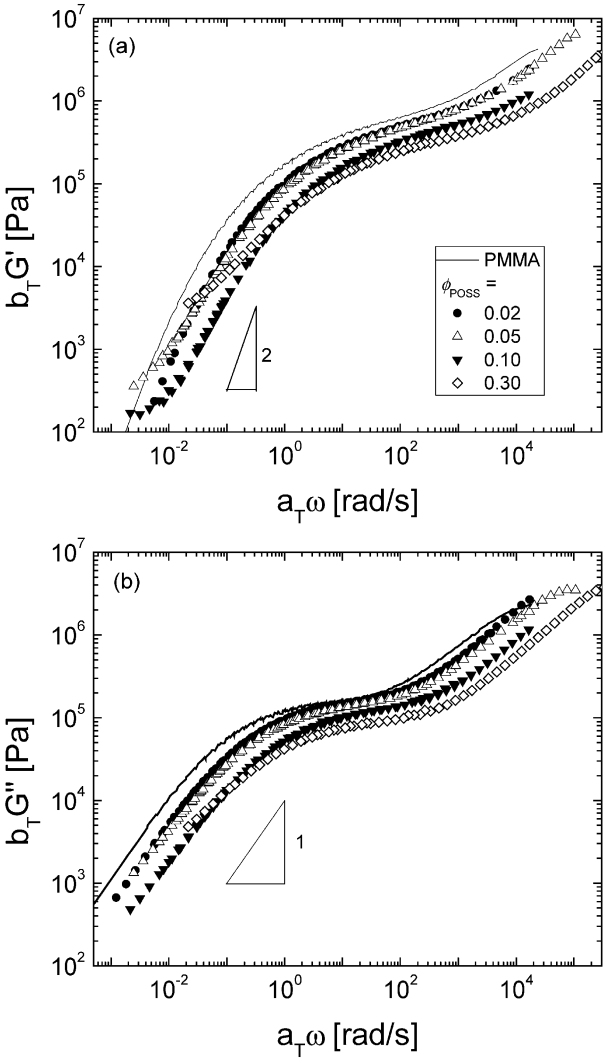

Fig. 5. Master curves at $T_0 = 170$ °C for (a) the storage modulus G' and (b) the loss modulus G'' of unmodified acrylic-POSS–PMMA blends.

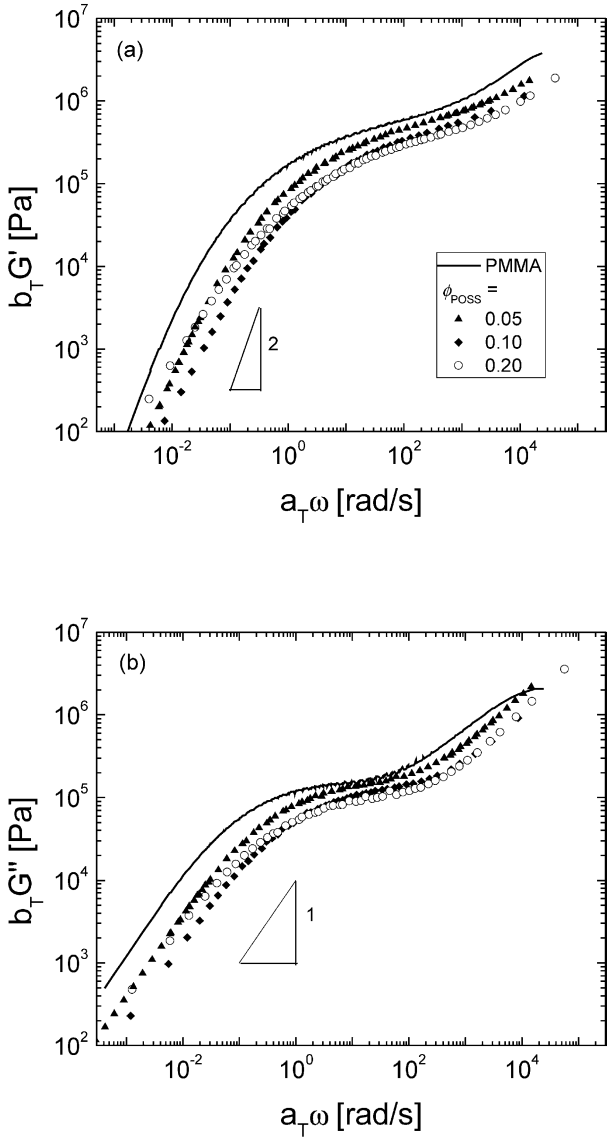

Fig. 6. Master curves at $T_0 = 170$ °C for (a) the storage modulus G' and (b) the loss modulus G'' of hydrogenated acrylic-POSS–PMMA blends.

$T_0 = 170$ °C. All blends closely followed the principles of time-temperature superposition (TTS) with a lateral shift $a_T(T,T_0)$ and a vertical shift $b_T(T,T_0)$ [31]. The addition of POSS causes significant shifts downward and to the right in the storage modulus $G'(\omega)$ and the loss modulus $G''(\omega)$. The shifts are greatest at loadings $\phi \leq 0.10$, which is also the region of steepest decrease in the T_g shown in Fig. 3. In the blends containing $\phi \geq 0.05$ unmodified acrylic-POSS in PMMA (Fig. 5), the storage modulus measured at low frequencies deviates from the characteristic terminal slope of 2 expected for simple viscoelastic fluids; this is caused by crosslinking of the pendant carbon–carbon double bonds on the unmodified acrylic-POSS. The $\phi = 0.05$ blend and the $\phi = 0.10$ blend begin to show crosslinking effects at a reduced frequency $a_T\omega \approx 10^{-2}$ rad/s, whereas the $\phi = 0.30$ blend shows this effect close to $a_T\omega \approx 10^{-1}$ rad/s. Samples containing $\phi \geq 0.05$ unmodified acrylic-POSS were placed in THF after rheological tests were performed. No soluble fraction was observed when the filtered solution was examined in GPC. The $\phi = 0.02$ blend does not show any effect of crosslinking in Fig. 5(a). The concentration dependence of the onset of crosslinking provides a clear indication that it is initiated by POSS–POSS contacts in the melt. At very low loadings ($\phi < 0.05$), POSS–POSS interparticle contacts are rare and thus no crosslinked network is formed; however, at higher loadings, the POSS cages contact each other regularly at high temperatures and are increasingly prone to react with each other to form a weakly crosslinked gel.

A common way to quantify the effect of a plasticizer on the linear viscoelastic properties of a polymer melt is with the relation [32]:

$$\frac{G_N^0\{\phi\}}{G_{N,\text{unfilled}}^0} = (1-\phi)^n \tag{3}$$

where $G_N^0\{\phi\}$ and $G_{N,unfilled}^0$ are the rubbery plateau moduli for a polymer containing a volume fraction ϕ of plasticizer and an unfilled polymer respectively, and the exponent n is a constant. The plateau modulus of the unfilled polymer ($G_{N,unfilled}^0$) was determined using the convention [33–35]:

$$G_N^0 = (G'(\omega))_{\tan\delta\to\min} \quad (4)$$

so that the plateau modulus is taken as the point along the storage modulus curve at which the loss tangent $\tan\delta = G''/G'$ passes through a minimum. To determine the plateau moduli of the POSS–PMMA blends, the storage modulus master curves for the blends were shifted manually by a horizontal factor a_ϕ and a vertical factor b_ϕ onto the G' curve of the unfilled polymer [32,36]. These shifted curves are shown in Fig. 7. The plateau modulus for each blend was then calculated as $G_N^0\{\phi\} = b_\phi G_{N,unfilled}^0$. These values of the plateau moduli are reported in Table 1. The quantity $-\log b_\phi$ is plotted against $-\log(1-\phi)$ in Fig. 8. The slope of the linear fit to these data is equal to the exponent n in Eq. (3). Many previous studies on polymer–plasticizer systems have reported values of n between 2.0 and 2.3 [32,37–40]. At POSS loadings $\phi \le 0.10$, the value of n is 2.47 ± 0.28 for the unmodified acrylic-POSS–PMMA blends and 2.24 ± 0.10 for the blends containing hydrogenated acrylic-POSS. These values are, within experimental error, similar to previous results for plasticized polymers. This volume fraction dependence of the plateau modulus on the POSS nanoparticle content is in contrast to the results obtained for the reduction of the glass transition temperature for POSS loadings $\phi \le 0.10$, where the reduction in the T_g was much less than that induced by the conventional plasticizer dioctyl phthalate. Above $\phi = 0.10$, the exponent n decreases significantly in the unmodified acrylic-POSS–PMMA blends to a value of 0.96 ± 0.05 due to the significant degree of phase separation of added POSS at these higher loadings.

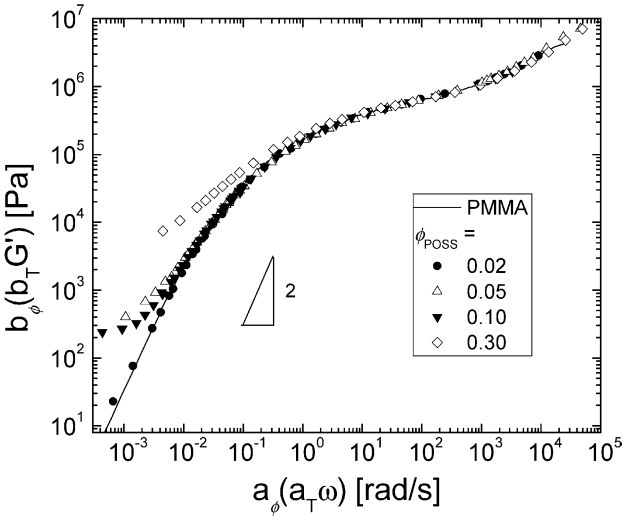

Fig. 7. Curves of the storage moduli for the unmodified acrylic-POSS–PMMA blends after applying horizontal (a_ϕ) and vertical (b_ϕ) concentration-dependent shift factors to superpose all curves onto the storage modulus curve of the unfilled homopolymer.

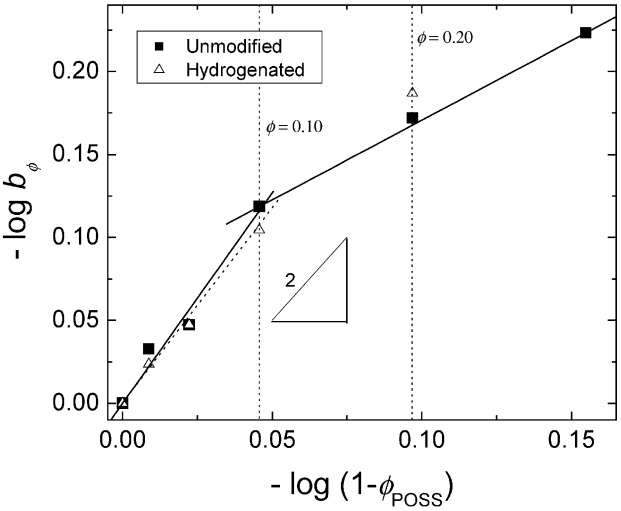

Fig. 8. A log–log plot of the horizontal shift factor $b_\phi = G_N^0\{\phi\}/G_{N,unfilled}^0$ against $(1-\phi_{POSS})$. The slope for conventional plasticizer–polymer systems typically lies between 2.0 and 2.3.

3.4. Time–temperature superposition and free volume

The TTS shift factors a_T obtained from the construction of the thermorheological master curves in Figs. 5 and 6 were analyzed using the WLF equation [31]:

$$\log a_T = \frac{-c_1^0(T - T_0)}{c_2^0 + (T - T_0)} \quad (5)$$

where c_1^0 and c_2^0 are constants and T_0 is the reference temperature. Values of the constants c_1^0 and c_2^0 were determined by plotting the quantity $-(T-T_0)/\log a_T$ against $(T-T_0)$; [31,41] the coefficient c_1^0 was obtained from the reciprocal of the slope, and the coefficient c_2^0 from the intercept. The WLF coefficients are reported in Table 1. The addition of unmodified acrylic-POSS leads to a strong decrease in c_1^0 and a significant increase in c_2^0. Similar trends are observed in the hydrogenated system, however the changes are less substantial. An important parameter that can be obtained from these fits is the fractional free volume f_0:

$$f_0 = \frac{B}{2.303 c_1^0} \quad (6)$$

where B is a constant usually assumed to be unity [31]. These fractional free volume values are plotted in Fig. 9. A clear trend is observed in the unmodified acrylic-POSS blend system. The free volume increases significantly for loadings $\phi \le 0.10$ and appears to asymptote towards a maximum value for $\phi \ge 0.20$.

The differential between the fractional free volume of the unfilled PMMA ($f_0 = 0.046$) and the $\phi = 0.05$ blend ($f_0 = 0.057$) is $\Delta f_0 = 0.011$, or 1.1×10^{19} nm^3/cm^3 of the blend. At

Table 1
Properties of methacryl-POSS–PMMA blends ($T_0 = 170$ °C)

vol% POSS	Hydrogenated	T_g (°C)	G_N^0 (Pa)	c_1^0	c_2^0 (K)	f_0/B	f_g/B
0		103.6	5.15×10^5	9.5	187	0.046	0.029
2	No	100.7	4.78×10^5	8.4	162	0.052	0.030
5	No	98.7	4.62×10^5	7.7	148	0.057	0.029
10	No	95.3	3.97×10^5	6.8	141	0.064	0.030
20	No	92.7	3.47×10^5	7.0	153	0.062	0.030
30	No	91.0	3.08×10^5				
5	Yes	100.1	4.62×10^5	9.3	189	0.046	0.029
10	Yes	97.9	4.05×10^5	8.1	173	0.053	0.031
20	Yes	98.0	3.35×10^5	8.4	172	0.052	0.030

$\phi = 0.05$, there are 2.32×10^{19} POSS molecules per cm^3 of the blend (assuming all T_{10} cages); from these values we may infer that the amount of free volume generated per added POSS molecule is 0.47 nm^3. The T_{10} acrylic-POSS cage has an approximate diameter of 2 nm, which corresponds to a hydrodynamic volume of 4.2 nm^3. The dense silica core, which contains 10 silicon atoms and 15 oxygen atoms, takes up less than 10% of this volume but contains 34% of the mass. Thus the volume of shell containing the acrylic R-groups is more than 3.5 nm^3. The density of the ten R-groups in this shell is approximately 0.45 g/cm^3, or half the bulk density of 0.9 g/cm^3 expected if the methacryloxypropyl R-groups were in their bulk state. This leaves approximately 1.75 nm^3 in the outer shell unfilled. The free volume increase per POSS molecule (0.47 nm^3) is approximately one-fourth this value and is quite reasonable when one considers the difficulty in fitting the relatively large polymer chains ($R_g \approx 15$ nm) into the small spaces between R-groups (<0.5 nm). The values of the fractional free volume plateau at $\phi = 0.20$ because the POSS phase-separates and begins to pack in its bulk amorphous configuration.

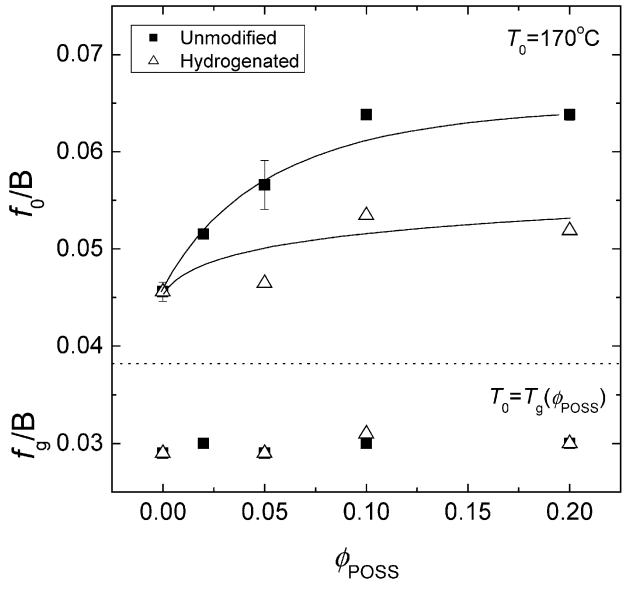

Fig. 9. Variation of the fractional free volume f_0/B with increasing volume fraction of POSS nanoparticles at a reference temperature $T_0 = 170$ °C. Also shown is the fractional free volume f_g/B at the glass transition temperature of each blend (Table 1). The error bars for the unfilled PMMA and the $\phi = 0.05$ blend in the unmodified acrylic-POSS system were determined by taking the standard deviation of three different samples.

The free volume data in Fig. 9 help clarify our previous results for PMMA filled with crystallizable-POSS species [13]. This earlier study reported that the POSS had a strong tendency to phase-separate into crystallites, even at loadings of $\phi = 0.01$, and we could not find a clear trend in free volume with increasing POSS content. The present data show that molecularly-dispersed POSS nanoparticles can plasticize PMMA by increasing the free volume within the matrix.

The fractional free volume f_0 at the reference temperature T_0 may be converted to the fractional free volume f_g at the glass transition temperature T_g using the relation [31]:

$$f_g = \frac{f_0(c_2^0 + T_g - T_0)}{c_2^0} \tag{7}$$

Values of f_g/B are listed in Table 1 and plotted at the bottom of Fig. 9. These values are approximately the same for all blends within experimental error. This indicates that, in these two blend systems, the glass transition is essentially an iso-free volume condition, and long-range molecular motion occurs only when the free volume reaches the same critical level regardless of blend composition. The differential increase in free volume $\Delta f_0(\phi)$ arising from the addition of POSS therefore serves to lower the temperature at which the total available free volume within the blends reaches this critical level, which is $f_g = 0.030 \pm 0.001$ for this set of PMMA-based materials. This result is in good agreement with the range of values reported by Ferry for conventional thermoplastics, which tend to fall in the range $0.025 \le f_g \le 0.035$ [31].

3.5. Dynamic mechanical analysis

We have shown that acrylic-POSS has a significant softening effect on the melt-state properties of PMMA (Figs. 5 and 6). The effect on the solid-state properties is also interesting in that it can reveal how the materials will behave at room temperature and below. Dynamic mechanical analysis was performed on the unmodified acrylic-POSS–PMMA

blends. The storage modulus E' and the loss tangent $\tan\delta = E''/E'$ measured at a frequency of 1 Hz are plotted as a function of temperature in Fig. 10. The trend observed in E' with increasing POSS loading is a decrease in the magnitude of the glassy modulus and a transition into the rubbery region at lower temperatures, consistent with a plasticizing effect.

When focusing more closely on the low temperature region $-80\,^{\circ}C \le T \le 0\,^{\circ}C$ [see inset to Fig. 10(a)], the effect of the plasticizer in the T_g region of the POSS can be observed. The $\phi = 0.05$ blend has a lower modulus than the unfilled PMMA but the two curves show no discernable difference in shape. The absence of any stiffening in the T_g region of the POSS is clear evidence that the POSS is dispersed on a molecular scale at a loading of $\phi = 0.05$. The $\phi = 0.10$ blend has the same value of the storage modulus as the $\phi = 0.05$ blend at $T = -80\,^{\circ}C$ but the modulus diverges to lower values as the temperature increases, indicating some aggregation of the POSS. The most significant difference is in the $\phi = 0.20$ blend, which has the highest modulus below the T_g of the POSS ($T_{g,POSS} = -55\,^{\circ}C$) but when the temperature is increased to $T = -25\,^{\circ}C$, it has the lowest modulus of any of the samples tested. This low temperature stiffening is caused by vitrified domains of phase-separated POSS that reinforce the sample like a rigid filler and make it stiffer than the pure matrix material. Above the T_g of the POSS, however, these hard POSS domains soften into sub-micron sized pools that reduce the stiffness of the material. Not surprisingly, this behavior also significantly affects the loss tangent E''/E' shown in Fig. 10(b). Not only is the β-relaxation of the PMMA shifted to lower temperatures with the addition of POSS, but in the glass transition region of the POSS, a conspicuous shoulder is present in the $\phi = 0.20$ blend.

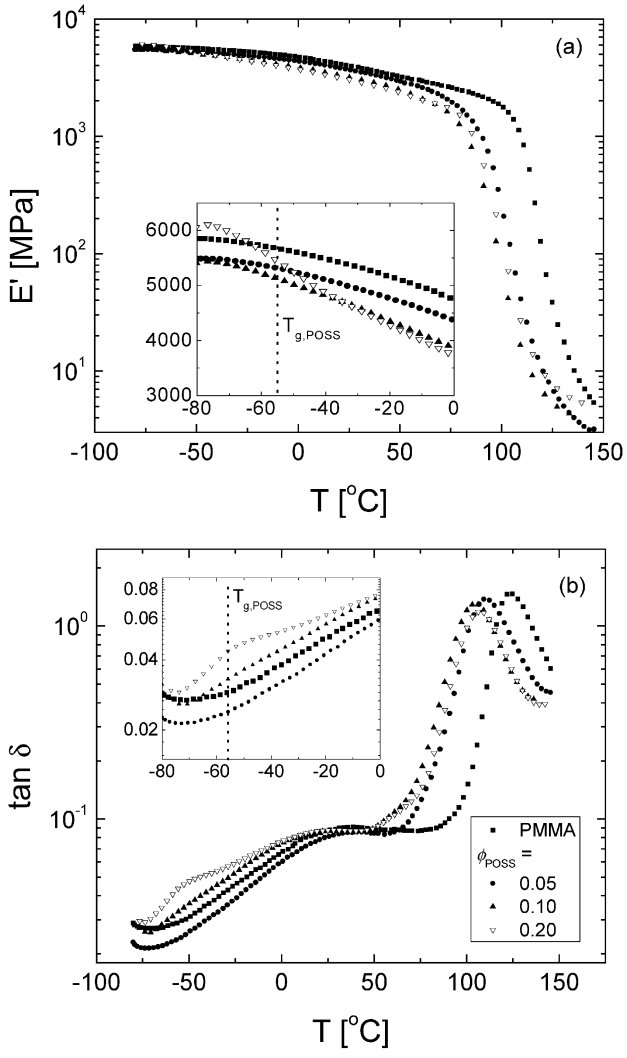

Fig. 10. DMA curves at a frequency of 1 Hz for (a) the storage modulus E' and (b) the loss tangent tan δ for blends of unmodified acrylic-POSS and PMMA.

4. Conclusions

Blends of poly(methyl methacrylate)(PMMA) with two acrylic polyhedral oligomeric silsesquioxanes (POSS) were analyzed to determine the effect of well-dispersed POSS nanoparticles on the thermomechanical properties of PMMA. Differential scanning calorimetry (DSC), dynamic mechanical analysis (DMA), and melt rheology all showed that POSS, when molecularly dispersed, behaved like a plasticizer. Differential scanning calorimetry (DSC) showed a larger drop in the glass transition temperature T_g in the blends containing unmodified acrylic-POSS ($\Delta T_g \approx 11\,^{\circ}C$ at $\phi_{POSS} = 0.20$) when compared with hydrogenated acrylic-POSS blends at the same loading ($\Delta T_g \approx 6\,^{\circ}C$). This difference in the degree of plasticization of the glass transition temperature depends on the degree of miscibility of the POSS and PMMA. Analysis of wide-angle X-ray diffraction patterns of both blend systems showed that significant phase separation of the POSS became apparent at loadings of $\phi \ge 0.20$.

Time temperature superposition (TTS) was successfully employed for all blends in order to construct thermorheological master curves and showed that the decrease in T_g was due to a substantial increase in the free volume of the blends. This plasticization resulted in a substantial decrease in the magnitude of the storage modulus G' and the loss modulus G'' in small amplitude oscillatory shear-flow. Analysis of the TTS data indicated that the free volume at the glass transition was virtually the same for all blends tested. Dynamic mechanical analysis of unmodified acrylic-POSS–PMMA blends showed a consistent decrease in the storage modulus with increasing POSS loading at room temperature; however, in the lower temperature range $-80\,^{\circ}C \le T \le 0\,^{\circ}C$ that brackets the T_g of the POSS ($T_{g,POSS} = -55\,^{\circ}C$), loadings of $\phi \ge 0.10$ showed evidence of a stiffening effect caused by vitrification of phase-separated POSS. No stiffening was observed in the $\phi = 0.05$ blend, indicating that molecular scale dispersion was

achieved at this loading in the unmodified acrylic-POSS–PMMA blends.

Acknowledgements

This research was sponsored by the DURINT project of the U.S. Air Force under grant F49620-01-1-0447. The use of the experimental facilities at MIT's Institute for Soldier Nanotechnologies is also greatly appreciated.

References

[1] Cole DH, Shull KR, Baldo P, Rehn L. Macromolecules 1999;32:771.
[2] Glotzer SC. Nat Mater 2003;2:713.
[3] Mackay ME, Dao TT, Tuteja A, Ho DL, Van Horn B, Kim HC, et al. Nat Mater 2003;2:762.
[4] McCoy JD, Curro JG. J Chem Phys 2002;116:9154.
[5] Roberts C, Cosgrove T, Schmidt RG, Gordon GV. Macromolecules 2001;34:538.
[6] Zhang Q, Archer LA. Langmuir 2002;18:10435.
[7] Starr FW, Schroder TB, Glotzer SC. Phys Rev E 2001;64:021802.
[8] Starr FW, Schroder TB, Glotzer SC. Macromolecules 2002;35:4481.
[9] Phillips SH, Haddad TS, Tomczak SJ. Curr Opin Solid State Mater Sci 2004;8:21.
[10] Carroll JB, Waddon AJ, Nakade H, Rotello VM. Macromolecules 2003;36:6289.
[11] Gonzalez RI, Phillips SH, Hoflund GB. J Spacecraft Rockets 2000;37:463.
[12] Huang JC, He CB, Xiao Y, Mya KY, Dai J, Siow YP. Polymer 2003;44:4491.
[13] Kopesky ET, Haddad TS, Cohen RE, McKinley GH. Macromolecules 2004;37:8992.
[14] Romo-Uribe A, Mather PT, Haddad TS, Lichtenhan JD. J Polym Sci, Part B: Polym Phys 1998;36:1857.
[15] Xu H, Kuo SW, Chang FC. Polym Bull 2002;48:469.
[16] Zheng L, Farris RJ, Coughlin EB. Macromolecules 2001;34:8034.
[17] Zheng L, Hong S, Cardoen G, Burgaz E, Gido SP, Coughlin EB. Macromolecules 2004;87:8606.
[18] Zheng L, Waddon AJ, Farris RJ, Coughlin EB. Macromolecules 2002;35:2375.
[19] Waddon AJ, Coughlin EB. Chem Mater 2003;15:4555.
[20] Waddon AJ, Zheng L, Farris RJ, Coughlin EB. Nano Lett 2002;2:1149.
[21] Mather PT, Jeon HG, Romo-Uribe A, Haddad TS, Lichtenhan JD. Macromolecules 1999;32:1194.
[22] Larsson K. Arkiv Kemi 1960;16:209.
[23] Hsiao BS, White H, Rafailovich M, Mather PT, Jeon HG, Phillips S, et al. Polym Int 2000;49:437.
[24] Constable GS, Lesser AJ, Coughlin EB. Macromolecules 2004;37:1276.
[25] Barry AJ, Daudt WH, Domicone JJ, Gilkey JW. J Am Chem Soc 1955;77:4248.
[26] Kim GM, Qin H, Fang X, Sun FC, Mather PT. J Polym Sci, Part B: Polym Phys 2003;41:3299.
[27] Zhang WH, et al. Macromolecules 2002;35:8029.
[28] Lamm MH, Chen T, Glotzer SC. Nano Lett 2003;3:989.
[29] Fu BX, Gelfer MY, Hsiao BS, Phillips S, Viers B, Blanski R, et al. Polymer 2003;44:1499.
[30] Fox TG. Bull Am Phys Soc 1956;1:123.
[31] Ferry JD. Viscoelastic properties of polymers. New York: Wiley; 1980.
[32] Nakajima N, Varkey JP. J Appl Polym Sci 1998;69:1727.
[33] Lomellini P, Lavagnini L. Rheol Acta 1992;31:175.
[34] Wu S. J Polym Sci, Part B: Polym Phys 1989;27:723.
[35] Fuchs K, Friedrich C, Weese J. Macromolecules 1996;29:5893.
[36] Graessley WW. Adv Polym Sci 1974;16:133.
[37] Nakajima N, Varkey JP. Polym Int 1998;46:298.
[38] Raju VR, Menezes EV, Marin G, Graessley WW, Fetters LJ. Macromolecules 1981;14:1668.
[39] Colby RH, Fetters LJ, Funk WG, Graessley WW. Macromolecules 1991;24:3873.
[40] Isono Y, Fujimoto T, Takeno N, Kjiura H, Nagasawa M. Macromolecules 1978;11:888.
[41] Fetters LJ, Graessley WW, Kiss AD. Macromolecules 1991;24:3136.